Nuclear Engineering and Technology 57 (2025) 103508

Contents lists available at ScienceDirect

Nuclear Engineering and Technology

journal homepage: www.elsevier.com/locate/net

Original Article

An approach to develop real-time in-situ underwater monitoring system based on integrated beta and gamma detection

Woo Nyun Choi [a,1], Min Ji Kim [b,1], Hyeonmin Lee [b], Seungbin Yoon [b], Hee Reyoung Kim [b,*]

[a] Doosan Enerbility, 22, DoosanVolvo-ro, Seongsan-gu, Changwon, Gyeongnam, 51711, Republic of Korea
[b] Department of Nuclear Engineering, Ulsan National Institute of Science and Technology (UNIST), 50 UNIST-gil, Ulju-gun, Ulsan, 44919, Republic of Korea

ARTICLE INFO

Keywords:
Monte-Carlo simulation
Disk source
On-site measurement
Organic scintillator
Inorganic scintillator

ABSTRACT

A real-time in-situ monitoring system for detecting beta and gamma nuclides underwater was proposed, and basic characteristic experiments were conducted. The current radiation monitoring system in Korea for low-energy beta nuclides uses liquid scintillation counting (LSC), which is time consuming and not recommended for rapid responses to uncontrolled releases.

An integrated monitoring system comprising two scintillators (NaI(Tl) and plastic) was proposed and analyzed. This system exhibited gamma and beta detection efficiencies of 2.51 ± 0.025 % and 8.00 ± 0.08 %, respectively, for the ^{137}Cs and ^{90}Sr disk sources. The coincidence net count rates of ^{90}Sr from ^{90}Sr + ^{137}Cs were 578.00 ± 0.58 and 577.06 ± 0.77 cps, respectively. The system revealed a relative difference of 0.40 %, which eliminated the effect of gamma nuclide, thus providing a methodological basis for distinguishing between underwater beta and gamma nuclides. The results indicated that the present approach could be usefully applied to establish a real-time beta and gamma monitoring system for underwater environments, such as groundwater at decommissioning sites.

1. Introduction

Radioactive materials generated during the operation of nuclear power plants (NPPs) and other nuclear facilities are released into the external environment within legally acceptable limits. Such releases should be meticulously planned according to the procedures outlined in technical guidelines for NPP operations. Planned releases ensure that radioactivity levels do not reach thresholds that would endanger the environment and surrounding communities. Additionally, the radiation dose from NPPs should be maintained as low as reasonably achievable to ensure public safety. However, in some decommissioned or currently operational NPPs in the United States—such as the decommissioned Indian Point NPP and the currently operational Braidwood NPP—radioactive materials were unintentionally released due to system or equipment leaks or operator errors, resulting in groundwater contamination [1,2]. Unlike planned releases, uncontrolled releases do not follow a pre-determined route, meaning radioactive materials may reach the environment without being monitored or controlled. Therefore, NPP operators must proactively prevent uncontrolled releases. Given the diverse causes of such releases and the challenge of completely preventing them, early detection and prompt response mechanisms are crucial.

On-site groundwater should be regularly monitored before and after the decontamination and decommissioning (D&D) of nuclear facilities, including early monitoring of uncontrolled releases. If releases are controlled following the remediation of a D&D site, long-term groundwater radiation monitoring is required. Beta nuclides generated from nuclear facilities must be managed from the perspective of health physics, necessitating technology capable of promptly and accurately detecting the contamination levels.

In Korea, environmental radioactivity around nuclear facilities is currently assessed according to the Korea Nuclear Safety and Security Commission notice No. 2017-17, "Regulations on Environmental Radiation Monitoring and Environmental Radiation Impact Assessment around Nuclear Facilities" [3]. Water samples, including rainwater, surface water, and groundwater, were collected monthly for environmental radiation monitoring [4]. These samples were analyzed for gross-beta radiation, tritium, and gamma radiation. However, measuring instruments such as liquid scintillation counters (LSC) require pretreatment due to the short range of low-energy beta nuclides,

* Corresponding author.
E-mail address: kimhr@unist.ac.kr (H.R. Kim).
[1] These authors contributed equally to this work.

https://doi.org/10.1016/j.net.2025.103508
Received 1 June 2024; Received in revised form 23 January 2025; Accepted 23 January 2025
Available online 24 January 2025

making in-situ LSC impractical if long sampling and analysis times are needed [4]. Consequently, prompt response to uncontrolled conditions is challenging.

Real-time in-situ gross beta measurements in underwater environments are not currently practiced in Korea. Consequently, efforts were made to develop an in-situ beta measurement system for use at D&D sites was attempted [5]. Plastic scintillators, known for their high sensitivity to short range beta particles and minimal damage upon contact with water, form the basis of this system [5]. A system was proposed for monitoring short-range beta radiation in groundwater at D&D sites. For existing groundwater in-situ beta measurement systems, which measure ^{3}H and ^{90}Sr, additional studies are required to determine whether water samples contain gamma nuclides. To address this, a detector using an inorganic scintillator was added. This study focuses not only on detecting gamma nuclides but also on determining beta coincidence counts while minimizing the effects of gamma nuclides in water samples.

2. Material and methods

2.1. Detection system

2.1.1. Beta-detection system

Plastic scintillators are physically and chemically stable even when in direct contact with water. Additionally, owing to their low effective atomic number, they exhibit minimal backscattering and low sensitivity to gamma rays, which helps reduce background levels. Leveraging the characteristics of short-range beta particles in water and the non-hygroscopic nature of plastic scintillators, a detection system was designed to detect short-range particles when they are in direct contact with the plastic scintillator, as depicted in Fig. 1 [6]. The monitoring system was also designed for real-time monitoring by circulating water samples through the system via a pump, similar to methods used in existing studies [5].

A plastic scintillator (EJ-212, Eljen Technology) was used for beta detection. The material properties of EJ-212 are listed in Table 1 [7]. The maximum emission wavelength of the EJ-212 scintillator is 423 nm, which is similar to the wavelength of the PMT R878 (Hamamatsu) used in this study, which has a peak emission at 420 nm.

The PMT R878, a head-on type photomultiplier tube [8], was selected for its suitable size for laboratory-scale experiments and cost-effectiveness in implementing a monitoring system. As listed in Table 2 [8], the PMT R878 has an effective area with a diameter of 46 mm and is supplied with 1250 V from a high-voltage power supply. It covers the 300–650 nm range with a peak.

2.1.2. Gamma-detection system

Inorganic scintillators with high atomic numbers and densities are typically used for gamma-ray measurements. Most of these scintillators consist of a single transparent material, varying in size from a few millimeters to several centimeters. They offer extremely high light output and detection efficiency for gamma rays [9]. For instance, NaI(Tl), an inorganic scintillator, has light output and absolute detection efficiency approximately four times greater than those of common plastic scintillators. However, many inorganic scintillators with high light output have relatively long decay times. The decay time affects the time resolution, crucial for the simultaneous counting methods used in this study. Longer decay times can degrade time resolution and increase random simultaneous counting signals, which are considered background radiation and can obscure the actual sample signals, especially in environments with high background radiation. Therefore, the decay time of inorganic scintillators is a critical factor. Additionally, hygroscopicity is an important consideration for in-situ underwater monitoring. This study evaluated NaI(Tl), GAGG(Ce), $LaBr_3$, and $CeBr_3$ as potential candidates. Table 3 lists the properties of these scintillators [10–14]. Among them, $LaBr_3$(Ce) and $CeBr_3$ demonstrated the best decay times of 25 ns and 19 ns, respectively, whereas GAGG(Ce) presented an intermediate decay time. The light yield, which is directly proportional to detection efficiency, is above 40,000 photons/MeV for most candidates. Notably, GAGG(Ce) is the only candidate that is resistant to hygroscopicity.

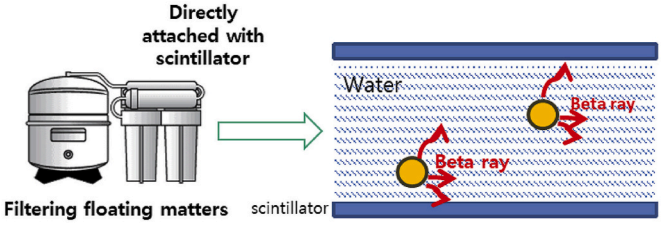

Fig. 1. Concept of the in-situ beta monitoring system using plastic scintillators [6].

Table 1
Properties of EJ-212 (Eljen technology) [7].

Properties	EJ-212
Light output [% anthracene]	65
Scintillation efficiency [photons/1 MeV e^-]	10,000
Wavelength of maximum emission [nm]	423
Light-attenuation length [cm]	250
Rise time [ns]	0.9
Decay time [ns]	2.4
Full width at half maximum (FWHM) [ns]	2.7
No. of H atoms per cm^3 [$\times 10^{22}$]	5.17
No. of C atoms per cm^3 [$\times 10^{22}$]	4.69
Density [g/cm^3]	1.023
Polymer base	PVT
Refractive index	1.58

Table 2
Specifications of PMT R878 [8].

Type	Head-on type
Tube size	Dia. 51 mm
Photocathode area shape	Round
Photocathode area size	Dia. 46 mm
Wavelength (short) [nm]	300
Wavelength (long) [nm]	650
Wavelength (peak) [nm]	420
Photocathode material	Bi-alkali
Window material	Borosilicate glass
Anode-to-cathode supply voltage [V]	1250
Time response (rise time Typ.) [ns]	7
Time response (transit time Typ.) [ns]	70

2.2. Monte-Carlo simulation

To evaluate the energy-specific detection efficiency based on scintillator thickness and sample temperature, a Monte-Carlo simulation using MCNP6.2 was performed [15]. Fig. 2 illustrates the MCNP6.2 modeling, which was conducted to derive the beta- and gamma-detection characteristics. The NaI scintillator was encapsulated in an aluminum cell, with magnesium oxide (MgO) used as a reflector. Due to the NaI scintillator's susceptibility to mechanical and thermal shocks and its deliquescence, it was sealed with an aluminum cell [16]. The MgO reflector had a thickness of 1.85 mm, and the aluminum packaging was 0.5 mm thick. The NaI scintillator was modeled as a cylinder with a diameter and height of 5.08 cm. The water sample was contained within a 5 cm cube, excluding the acrylic structure supporting the EJ-212. The material of the detection section containing the water sample was modeled as a 6 cm cube. The detector size was determined by optimizing the diameter of the R878 used in this study (5 cm). Consequently, the diameter of the EJ-212 was also 5 cm, and a hole with

Table 3
Properties of four inorganic scintillator candidates [10–14].

Materials	Density [g/cm^3]	Wavelength of maximum emission [nm]	Principal decay constant [μs]	Total light yield [photons/MeV]	Hygroscopicity
NaI(Tl)	3.67	415	0.23	55,000	O
GAGG(Ce)	6.63	520	0.05–0.15	40,000–60,000	X
$LaBr_3$	5.08	380	0.02	60,000	O
$CeBr_3$	5.2	380	0.02	60,000	O

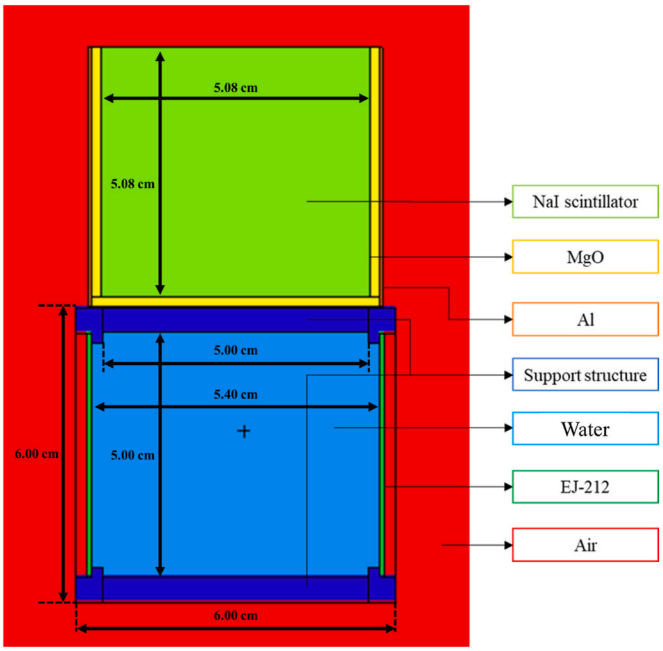

Fig. 2. MCNP6 modeling of the beta and gamma monitoring detector (front view).

a diameter of 4.6 cm was modeled to accommodate it.

2.2.1. Beta- and gamma-detection efficiency based on plastic-scintillator thickness

The beta-detection efficiency based on the plastic-scintillator thickness was calculated using MCNP6.2. As depicted in Fig. 3, the modeling was performed on EJ-212 plastic scintillators with thickness of 1, 3, and 5 mm. The beta-detection efficiency was evaluated using ^{3}H, ^{14}C, and ^{90}Sr sources. For gamma-detection efficiency, the source was modeled to emit monoenergetic gamma rays with energy levels of 0.05, 0.1, 0.2, 0.5, 0.8, 1.0, 1.5, 2.0, 2.5, and 3.0 MeV. Additionally, the source was homogeneously distributed within the water samples.

2.2.2. Beta- and gamma-detection efficiency based on inorganic-scintillator thickness

To evaluate the energy-specific detection efficiency based on the inorganic-scintillator thickness, a Monte-Carlo simulation using MCNP6.2 was performed. The source was homogeneously distributed within the water samples. For assessing beta radiation detection efficiency, the source was modeled as ^{90}Sr, which emits high-energy beta radiation. For evaluating energy-detection efficiency, the source emitted monoenergetic gamma rays at energy levels of 0.05, 0.1, 0.2, 0.5, 0.8, 1.0, 1.5, 2.0, 2.5, and 3.0 MeV. To evaluate the optimal thickness, the range of high detection efficiency was determined by varying the thickness from 1 to 7 cm in 1 cm increments. This range was chosen to account for attenuation in thicker scintillators and to exclude thicknesses in millimeters where interaction probabilities were low. Note that MCNP6.2 does not account for the scintillation process; instead, the detection efficiency was determined based on the number of gamma rays deposited on the scintillator, using the F8 tally. The detection-efficiency results obtained from the simulations were calculated using Equation (1).

$$\varepsilon_{MC} = \frac{\text{Peak number of photons in the simulated spectrum}}{\text{Number of photons emitted by the source}}. \quad (1)$$

2.3. Design of detection circuit

Coincidence counts for gross-beta detection were obtained as illustrated in the conceptual schematic in Fig. 4. To acquire the incident radiation signal, a high-voltage power supply (556, ORTEC) provided the operating voltage to the PMT [17]. The two output signals of the PMT were simultaneously amplified using a dual amplifier (855, ORTEC) [18]. A timing single-channel analyzer (SCA; 551, ORTEC) and a time-to-amplitude converter (567, ORTEC) were used in the coincidence method to minimize the background effect [19–21]. The signal acquired from the coincidence method was digitized using a multichannel analyzer (EASY-MCA 2 K, ORTEC) [22]. For acquiring the energy spectra of gamma nuclides, the same high-voltage power supply (556, ORTEC), amplifier (855, ORTEC), and MCA (EASY-MCA 2 K, ORTEC) were used.

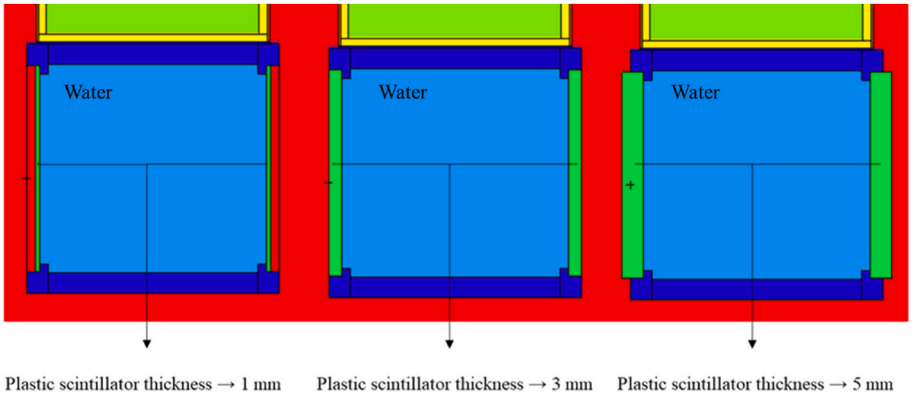

Fig. 3. MCNP6 modeling based on plastic scintillator thickness.

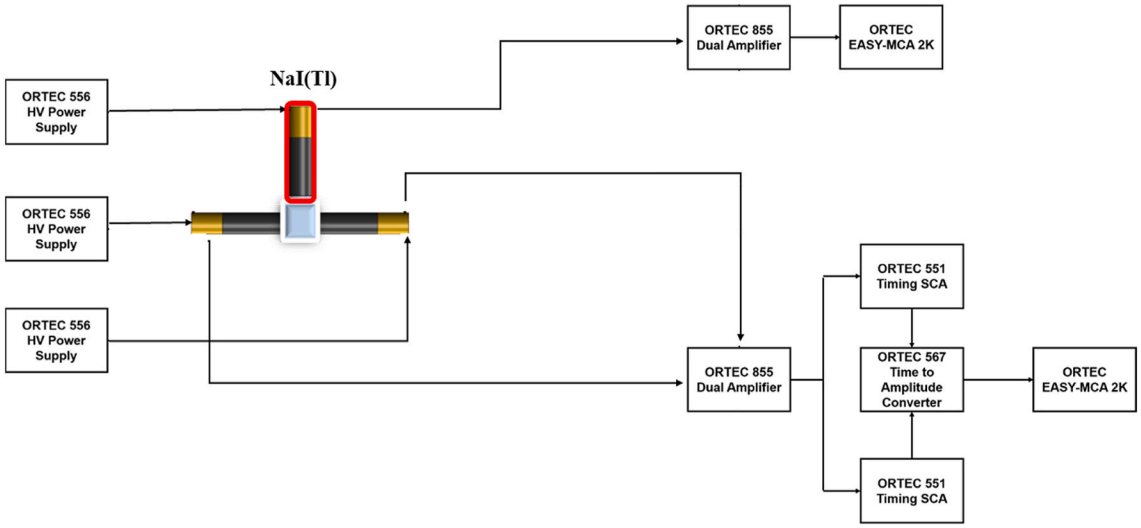

Fig. 4. Schematic illustration of the conceptually designed gross-beta coincidence-count detection system.

2.4. Derivation of gross-beta detection efficiency using disk sources

A verification experiment was performed using disk sources in air to validate the method of deriving beta and gamma radioactivity with the monitoring system before applying it to water samples. For beta measurements, a ^{90}Sr disk source was used, while ^{60}Co and ^{137}Cs disk sources were used for gamma measurements. ^{60}Co and ^{137}Cs were the main nuclides analyzed in the water samples. The experiment utilized ^{90}Sr as a representative gross-beta source due to its extensive use as a standard for gross-beta activity and its higher decay energy of 546 keV compared to other beta sources [23]. ^{90}Sr is in radioactive equilibrium with its daughter nuclide ^{90}Y. The parameters of the disk sources used to derive detection efficiency are listed in Table 4. The experiments with disk sources were performed in July 2023. The experimental setup for measuring gross-beta detection efficiency is shown in Fig. 5, and the overall process is illustrated in Fig. 6. The combined uncertainty for the full energy peak efficiency (FEPE) of ^{137}Cs and the detection efficiency of ^{90}Sr includes the uncertainties in source radioactivity, full peak emission probability, and counting measurement.

2.4.1. Calibration of NaI(Tl) detector, derivation of ^{137}Cs FEPE, and coincidence counts using disk sources

The disk sources used for the calibration of the NaI(Tl) detector were ^{60}Co and ^{137}Cs. A schematic illustration of the experimental setup is depicted in Fig. 7. The spectrum was derived using MCA by connecting the PMT to an 855 dual amplifier using a NaI(Tl) scintillator that was not affected by beta as a scintillator-support structure. The coarse gain of the 855 dual amplifier was set to 20, and the fine gain was set to 6.5 for the NaI(Tl) scintillator. The measurement time was 900 s.

To calibrate the NaI(Tl) detector, the absolute FEPE was derived from the gamma energy spectrum of the source. The FEPE is calculated as shown in Equation (2). Following this, the environment was simulated using MCNP6.2, and the results from the simulation were compared and analyzed against the experimental data.

Table 4
Parameters of disk sources used for detecting efficiency.

Parameters	^{90}Sr/^{90}Y	^{60}Co	^{137}Cs
Original activity [kBq]	3.7/3.7	37	9.25
Production date	2022.07.12	2022.07.14	2022.07.12
Half-life	28.78 y/64 h	5.27 y	30.08 y
Manufacturer	Spectrum Techniques (TN)		

$$\varepsilon_{Exp} = \frac{A}{S \times P(E) \times t} \tag{2}$$

A = Full energy peak area count of source
S = Activity of source (Bq)
$P(E)$ = Probability of gamma ray with energy E being emitted
t = Measurement time (live time) (s)

Additionally, the effect of the beta source ^{90}Sr on the NaI(Tl) detection system was evaluated. The same experimental settings as those depicted in Fig. 7 were configured, and the energy spectra of the ^{90}Sr disk source and background were derived and analyzed.

Thereafter, the coincidence counts of ^{137}Cs were derived using two plastic scintillators. Net counts were derived by excluding background counts from the gross counts of ^{137}Cs, and the detection efficiency was derived based on the net counts of ^{137}Cs. A schematic illustration of the experiment performed to derive the coincidence counts for ^{137}Cs is depicted in Fig. 8. The scintillation signals generated by the interaction between each plastic scintillator and ^{137}Cs were amplified using an amplifier. These signals were then input to different timing SCAs for conversion into timing signals. If two timing signals occurred within the time window defined by the 567 time-to-amplitude converter, they were processed as coincidence counts. In this experiment, the coarse gain of the amplifier was set to 20 and the fine gain to 2.5. For the 551 timing SCA, the lower level was set to 0.1, and the time window of the 567 time-to-amplitude converter was set to 20 μs. The measurement duration was 1800 s.

2.4.2. Derivation of beta and gamma coincidence counts and gross-beta detection efficiency using disk sources

Coincidence counts for ^{90}Sr and ^{90}Sr + ^{137}Cs disk sources were derived under identical experimental conditions, as depicted in Fig. 8. First, the FEPE for ^{90}Sr + ^{137}Cs disk sources was determined using a NaI (Tl) detector and compared with the FEPE for ^{137}Cs alone, as depicted in Fig. 7. The activity of ^{137}Cs was calculated from its FEPE value obtained with the NaI(Tl) detector. The coincidence counts for ^{137}Cs were calculated using the detection efficiency value of ^{137}Cs for the plastic scintillators, as detailed in Section 2.4.1, based on the derived activity of ^{137}Cs. To verify the detection system, the coincidence counts for ^{137}Cs were subtracted from the coincidence counts for ^{90}Sr + ^{137}Cs disk sources. The resulting values were then compared with the coincidence counts for ^{90}Sr disk sources.

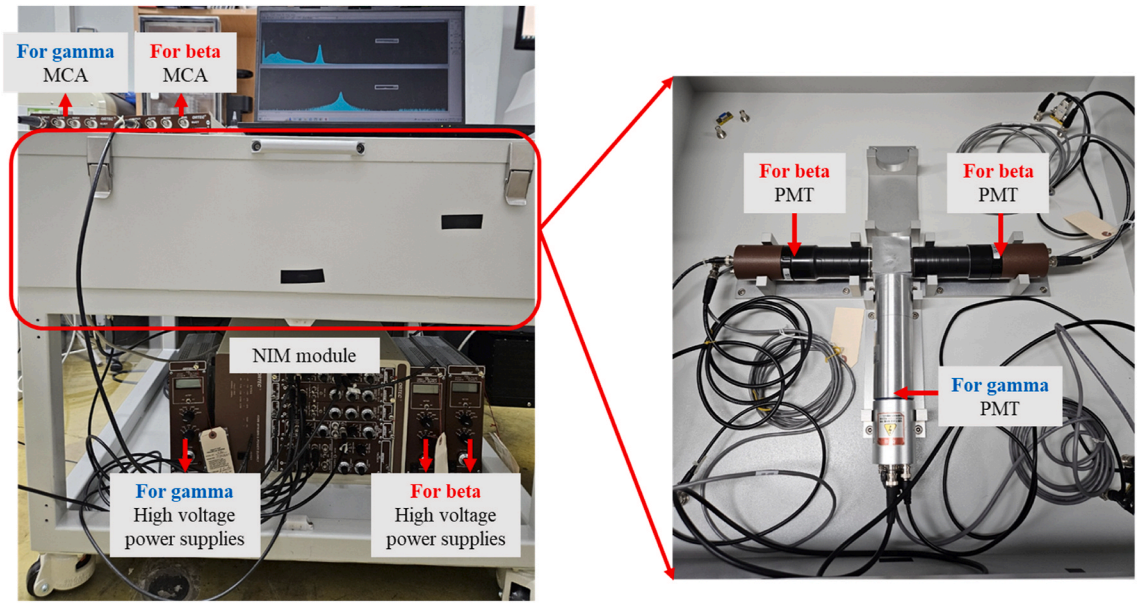

Fig. 5. Experimental setup.

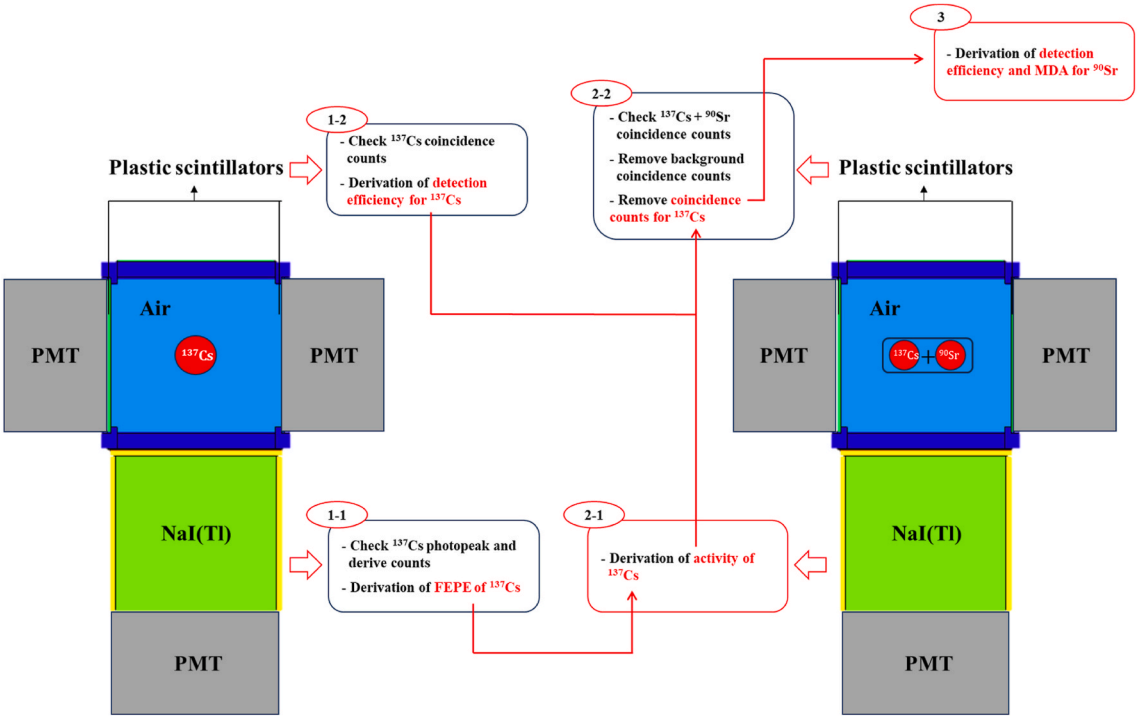

Fig. 6. Schematic illustration of the verification method for deriving gross-beta efficiency using disk sources.

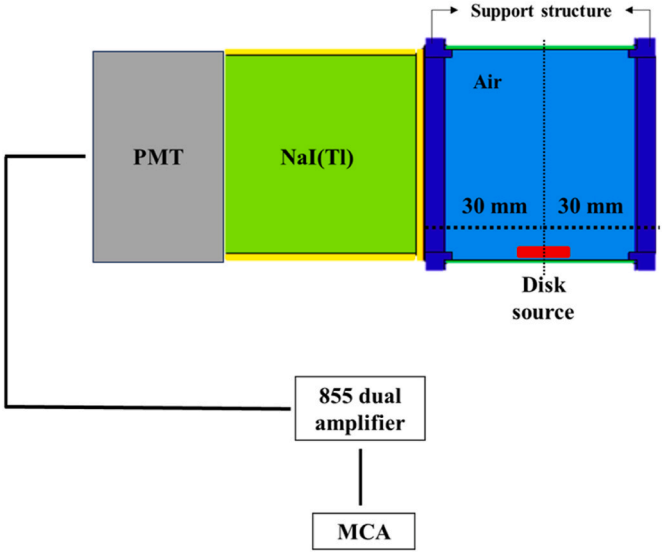

Fig. 7. Schematic illustration for deriving the gamma energy spectrum.

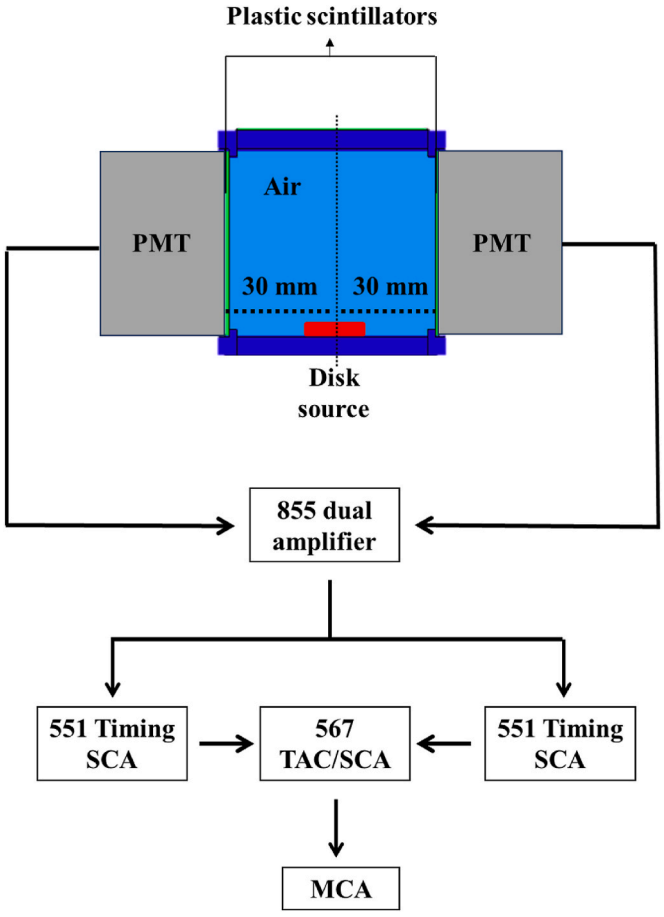

Fig. 8. Schematic illustration for deriving the coincidence count of the gamma source.

Table 5
Detection efficiencies of 1-, 3-, and 5-mm-thick plastic scintillators based on MCNP6 simulation.

	Detection efficiency of 1, 3, 5 mm scintillator (%)	Relative error (%)
^{3}H	0.0002	2.24
^{14}C	0.0021	0.68
^{90}Sr	0.1222	0.29

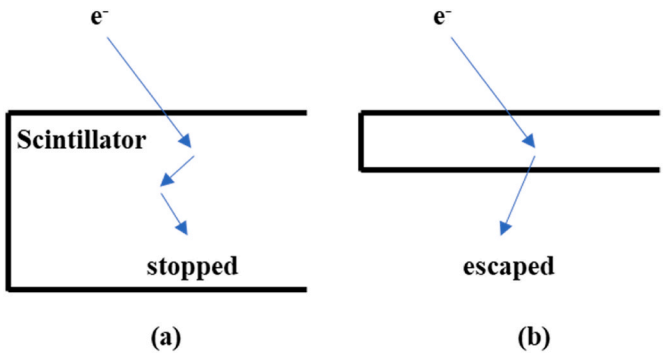

Fig. 9. Energy-deposition mechanism in MCNP simulation.

3. Results & discussions

3.1. Results of Monte-Carlo simulation

3.1.1. Beta- and gamma-detection efficiency based on plastic-scintillator thickness

By performing the MCNP simulation described in Section 2.2.1, the detection efficiencies of plastic scintillators measuring 1, 3, and 5 mm thick were determined, which were the same for the three thickness ranges, as shown in Table 5. Detection efficiencies of scintillators increase with the increase of the beta ray energy. The radionuclides were modeled to be contained within a water sample, where beta particles with short ranges are more likely to be absorbed by water before interacting with the scintillating material. This implies that low-energy beta particles lose a significant amount of their energy in water compared to high-energy beta particles, resulting in reduced interactions with the scintillating material and consequently lower detection efficiency. Based on the MCNP6.2 simulation results, the detection efficiency of the beta sources was not affected by the plastic-scintillator thickness. As shown in Fig. 9, the amounts of energy deposited for cases (a) and (b) are different; however, the nonzero energy deposition of beta particles in the scintillator in the F8 tally of MCNP6.2 was considered a count. As depicted in Fig. 10, the energy spectra of ^{3}H and ^{14}C were consistent, respectively, regardless of the different plastic-scintillator thickness and that of ^{90}Sr was consistent for the thicknesses of 3 and 5 mm. As the scintillator thickness increases from 1 mm to 5 mm, energy absorption reaches a saturation point, meaning that further increases in thickness do not significantly affect the results. However, the spectra appeared in the region of low energy not up to maximum energy, which was thought to be because the thickness of the specified cell was insufficient in MCNP simulation, causing most energetic electrons to be lost through transmission or other processes. Thin plastic scintillators reduce the self-absorption of photons generated during the scintillation process. Moreover, in gross-beta measurements, the 5-mm-thick plastic scintillator experienced relatively significant interference from gamma rays compared to the 1-mm-thick plastic

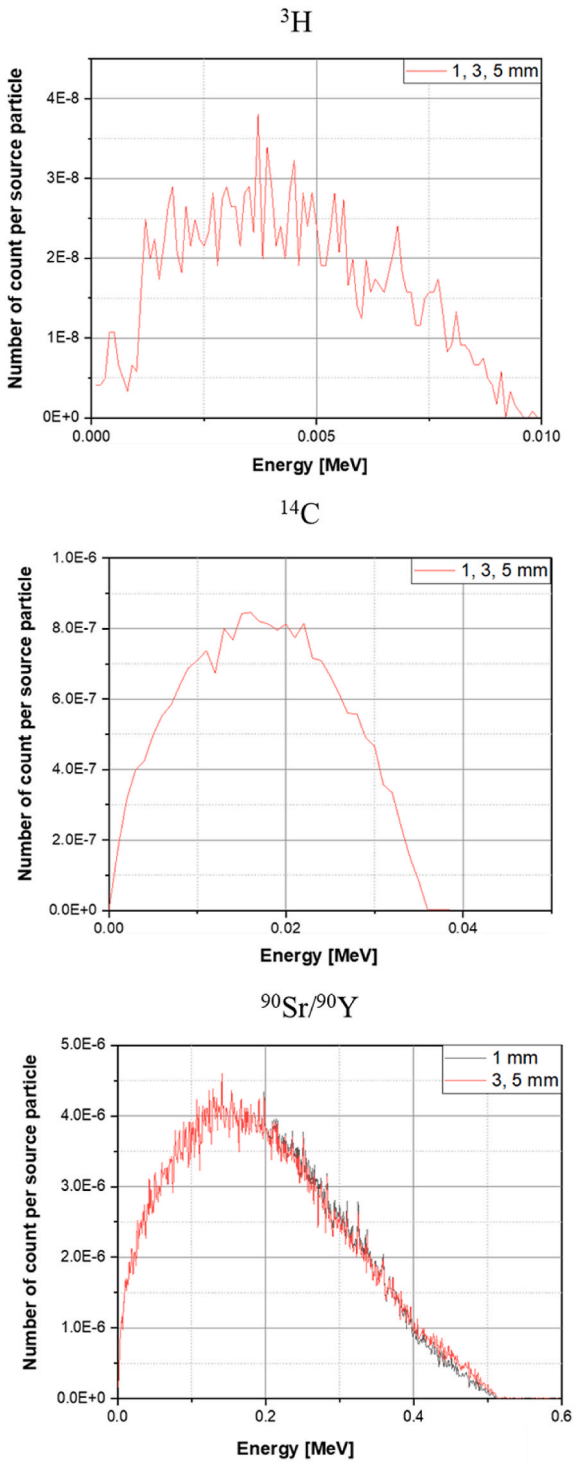

Fig. 10. Energy spectra of ^{3}H, ^{14}C, and ^{90}Sr.

scintillator. Consequently, among the 1, 3, and 5 mm plastic scintillators, the 1 mm scintillator was found to be the most suitable.

As depicted in Fig. 11, the effects of gamma rays on the 1, 3, and 5 mm plastic scintillators were derived using MCNP6.2. As shown in Fig. 11, the spectrum of a plastic scintillator reflects energy deposition, resulting in a combined shape of the Compton continuum and double escape peaks for the range of given gamma-ray energy. All graphs exhibited similar trends, regardless of the plastic scintillator thickness.

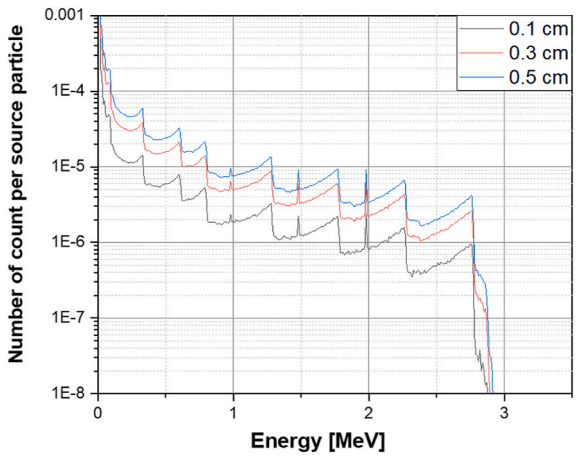

Fig. 11. Energy spectra of gamma rays based on plastic-scintillator thickness.

The results confirmed that the influence of gamma rays increased with the plastic-scintillator thickness. This is because thinner plastic scintillators allow greater penetration of gamma rays. Additionally, the findings confirmed that a thinner plastic scintillator could minimize the impact of gamma rays. However, as the thickness decreases, the risk of physical damage increases due to direct contact with the sample.

3.1.2. Beta- and gamma-detection efficiency based on inorganic-scintillator thickness

In the case of beta rays, because of the support structure between the sample and scintillator, the beta rays could not reach the inorganic scintillator, thus resulting in zero detection efficiency in the MCNP6.2 simulation. This result is to be expected because only the gamma source should be detected in the beta–gamma mixed samples using an inorganic scintillator. Fig. 12 depicts the detection efficiency of each inorganic scintillator as a function of thickness, as obtained from the MCNP6.2 simulation. The results showed that the FEPE of GAGG(Ce) began to saturate at a thickness of 4 cm, whereas those of $LaBr_3$, $CeBr_3$, and NaI (Tl) began to saturate at a thickness of 5 cm. Saturation occurs when the increase in FEPE is less than 1 % with a 1 cm increase in scintillator thickness in the low-energy region. As thickness increased, the detection efficiency increased exponentially. Among the scintillator candidates, GAGG(Ce) exhibited the highest FEPE across most energy regions. However, GAGG(Ce) is less compatible when its maximum emission wavelength is 520 nm, given the most PMTs peak at a wavelength of 420 nm. The maximum emission wavelength of NaI(Tl) is 415 nm, which aligns best with the PMT used in this study. Consequently, a 5 cm NaI(Tl) scintillator was used in the experiment.

3.2. Results of gross-beta detection efficiency based on disk sources

3.2.1. Results of ^{137}Cs FEPE and coincidence counts using disk sources

The energy of the NaI(Tl) detector was calibrated to determine the FEPE of ^{137}Cs and to convert the number of channels into energy. Fig. 13 shows the energy-calibration curve based on the experimental data. The three full peaks were fitted using a linear function to establish the calibration function, which was determined using Equation (3). The R^2 value of the linear function was 1, indicating a perfect fit.

$$Y(\text{keV}) = 0.9442 \times X(\text{channel number}) + 31.814, \quad (3)$$

Fig. 14 compares the FEPE (ε_{Exp}) obtained experimentally with the detection efficiency obtained through simulations (ε_{MC}). The uncertainty in the FEPE was calculated by combining the uncertainties from the source radioactivity, full peak emission probability, and measurement counting. The experimentally derived FEPE for ^{137}Cs, was 2.51 ±

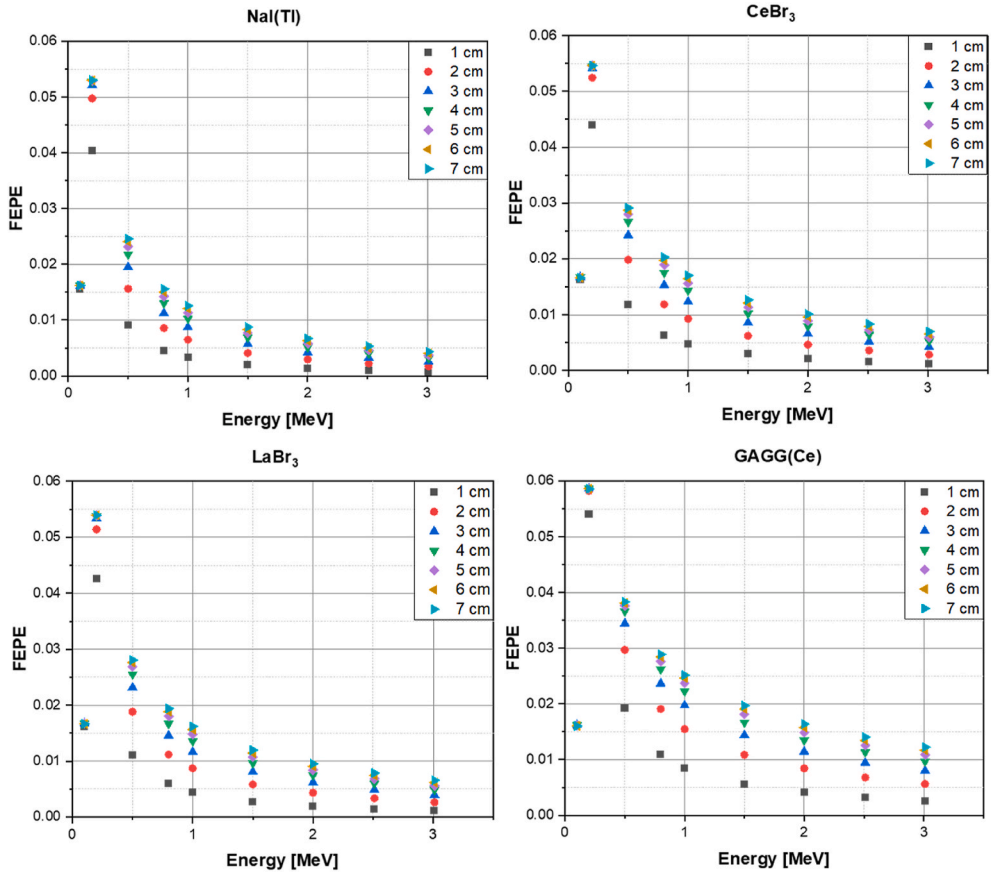

Fig. 12. Gamma-detection efficiencies based on organic-scintillator thickness.

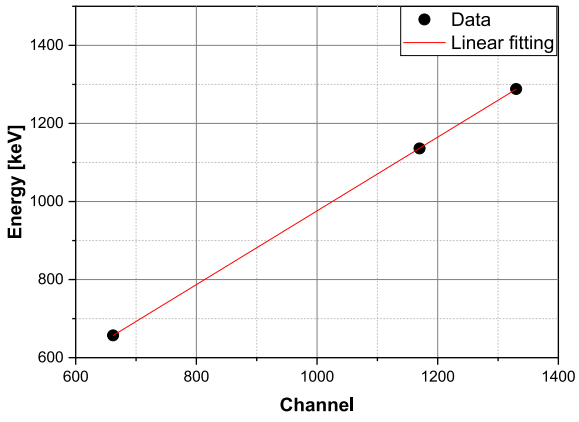

Fig. 13. Energy calibration of the NaI(Tl) detector.

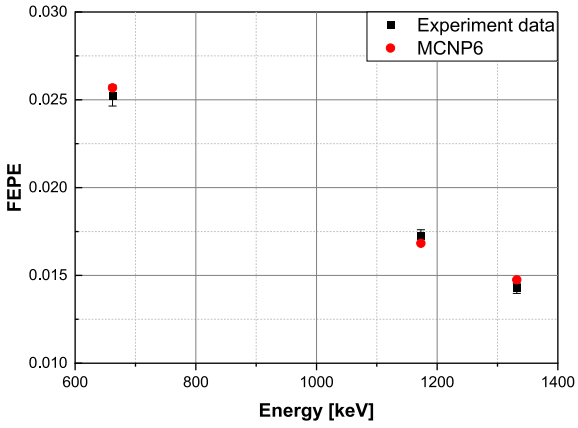

Fig. 14. Absolute full energy peak efficiency obtained from experiments and simulation.

0.025 %. For statistical evaluation, the relative difference between the measured data and the simulated data was assessed using Equation (4).

$$\text{Relative difference} = \frac{\text{measured data} - \text{simulation}}{\text{simulation}}\ [\%]. \quad (4)$$

The relative differences were 1.2 %–3.3 % compared with the MCNP6.2 results, thus indicating that MCNP6.2 agreed well with the measured data.

Fig. 15 depicts the ^{90}Sr and background energy spectra derived using the NaI(Tl) detection system. As depicted in the figure, the NaI(Tl) scintillator was not affected by the ^{90}Sr source. This is because beta rays have relatively low energy, which implies that they cannot penetrate the reflector or the aluminum that seals the NaI(Tl). These results confirmed that the FEPE for the gamma source can be derived using the NaI(Tl) detection system, even if a beta source existed in the sample.

Subsequently, the coincidence counts of ^{137}Cs were derived using the plastic scintillators. Table 6 lists the net coincidence count rate and detection efficiency of ^{137}Cs obtained with the plastic scintillators.

Assuming the disk source activity corresponds to ^{137}Cs, the activity

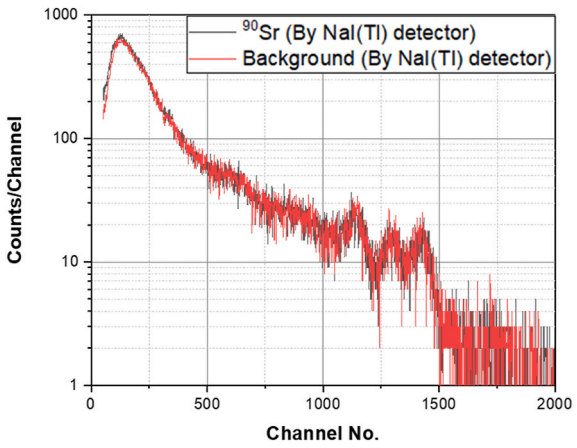

Fig. 15. ^{90}Sr and background energy spectra obtained using the NaI(Tl) detection system.

value of the sample can be determined using the 2.51 ± 0.025 % detection efficiency by counting the net area of the full peak with the NaI (Tl) detector. The net coincidence counts of ^{137}Cs can then be predicted using the desired activity value and the detection efficiency of 2.51 ± 0.025 % for the plastic scintillator. If the derived net coincidence counts exceed the expected value, the excess is likely attributable to gross-beta contributions.

3.2.2. Derivation of beta and gamma coincidence counts and gross-beta detection efficiency using disk sources

Table 7 lists net coincidence count rate and detection efficiency of ^{90}Sr when measuring only ^{90}Sr disk sources, as well as the net coincidence count rate when measuring both ^{90}Sr and ^{137}Cs disk sources together. The net coincidence count rate of the ^{90}Sr disk source measured in air using the plastic scintillator was 578.00 ± 0.58 cps, with a confirmed detection efficiency of 8.00 ± 0.08 %. By subtracting the net coincidence count rate of ^{137}Cs obtained in Section 3.2.1 from the net coincidence count rate of ^{90}Sr + ^{137}Cs disk sources, a value of 577.06 ± 0.77 cps was derived. The relative difference between these two net coincidence count rates was within a maximum of 0.40 %, where the effect of ^{137}Cs radioactivity was removed. As illustrated in the flowchart of Fig. 6, the coincidence counts for ^{137}Cs detected from a plastic scintillator detection system can be eliminated based on the radioactive activity of ^{137}Cs and its detection efficiency in the plastic scintillator system. Unlike the NaI(Tl) detection system, the plastic scintillator detects both gamma and beta radiation from ^{137}Cs. However, the detection efficiency of the plastic scintillator system is determined based on coincidence counts relative to the activity of ^{137}Cs during its characterization, inherently accounting for the combined effects of gamma and beta radiation. Therefore, by obtaining the radioactive activity of ^{137}Cs using the NaI(Tl) detection system, it is possible to subtract the influence of all ^{137}Cs radiation (gamma + beta) from the coincidence counts in the plastic scintillator detection system. Based on the disk-source experiments conducted in air, the procedure for deriving beta and gamma radioactivity using this monitoring system was successfully verified. However, because water has a higher attenuation coefficient than air, the detection efficiency for nuclides in water would be relatively lower compared to air. Despite this, the radioactivity of nuclides in water can be effectively separated using the detection efficiency-based approach for deriving the coincidence net count rate, as demonstrated in air. This approach leverages the detection efficiency evaluation of the integrated beta/gamma-detection monitoring system.

3.2.3. Derivation of minimum detectable activity (MDA) for ^{137}Cs and ^{90}Sr

The detector sensitivity describes how efficiently it converts radiation into a useable signal (i.e. "counts"). In other words, the sensitivity of a detector is defined by how small an amount of a sample it can measure for radioactivity. The MDA is calculated using Equation (5) [9]:

$$\mathrm{MDA} = \frac{2.71 + 4.65 \times \sqrt{n_b \times T}}{\mathrm{T} \times \mathrm{m} \times \varepsilon}\ [Bq/g]. \quad (5)$$

where n_b is background count rate [cps], T is sample and background count time [sec], m is sample mass [g], and ε is detection efficiency.

The MDA for ^{137}Cs of HPGe is 0.002–0.006 Bq/L for a measuring time of 80,000 s where it also depends on mass of the sample. The effluent control limit for ^{137}Cs is 50 Bq/L. In this monitoring system (sample amount 131.08 g, background counting rate 8.85 cps, measurement efficiency 2.51 %), a measurement time of approximately 7000 s is required to reach the effluent control limit. For gamma detection, this monitoring system does not require sensitivity up to HPGe as it is used to confirm the presence or absence of gamma nuclides and to eliminate their influence.

In this monitoring system, experiments were conducted on the beta radionuclide ^{90}Sr, and the MDA was compared for the low-background alpha/beta counter (LB), commercial device used to measure ^{90}Sr. The MDA for ^{90}Sr of LB is 0.2–0.4 mBq/L for a measuring time of 12,000 s. The effluent control limit for ^{90}Sr is 20 Bq/L. In this monitoring system (sample amount 131.08 g, background counting rate 8.85 cps, measurement efficiency 8.00 %), a measurement time of approximately 4000 s is required to reach the effluent control limit. The MDA of LB is much lower than that of this monitoring system. However, this monitoring system has the advantage of not requiring pre-treatment and allowing on-site measurement.

This analysis of beta radionuclides using HPGe and LSC typically takes 3–5 days from sample collection to preprocessing and measurement. However, this system can measure on-site without preprocessing, achieving MDA of 14.3 Bq/L for ^{137}Cs and 4.49 Bq/L for ^{90}Sr within 24

Table 6
Coincidence count and detection efficiency of ^{137}Cs.

	Background count rate [cps]	Gross count rate [cps]	Net count rate [cps]	Detection efficiency [%]
^{137}Cs	8.85 ± 0.07	239.70 ± 0.37	230.85 ± 0.37	2.51 ± 0.025

Table 7
Coincidence counts and detection efficiencies of ^{90}Sr and ^{90}Sr + ^{137}Cs and ^{90}Sr alone.

	Background count rate [cps]	Gross count rate [cps]	Net count rate [cps]	Detection efficiency [%]
^{90}Sr	8.85 ± 0.07	586.85 ± 0.57	578.00 ± 0.58	8.00 ± 0.08
^{90}Sr + ^{137}Cs	8.85 ± 0.07	816.76 ± 0.67	807.91 ± 0.68	–

h. These values correspond to 28.6 % and 22.5 % of effluent control limits, respectively. Accordingly, it is believed that this should be sufficient to determine whether there is contamination.

It was confirmed that the present experimental verification using disk sources could provide key information to the field applicability of a real-time in-situ beta and gamma monitoring system for water samples. If water samples are properly calibrated and the detection efficiency is accurately derived based on the source, the proposed system can be applied to various water types, including groundwater, seawater, and rainwater.

4. Conclusion

In this study, a continuous integrated beta/gamma-detection monitoring system was conceptually designed and evaluated for treating contaminated water from areas near nuclear facilities, such as decommissioning sites. The detection component was designed so that the sample was in direct contact with the plastic scintillator, enabling the detection of short-range beta nuclides in water. Additionally, MCNP 6.2 simulation was performed to evaluate NaI(Tl), GAGG(Ce), $LaBr_3$, and $CeBr_3$ inorganic scintillators, aiming to eliminate the influence of gamma nuclides if present in the sample. Based on the simulation results and PMT specifications, a 5-mm-thick NaI(Tl) scintillator was selected to construct the monitoring system.

The constructed gamma-detection system yielded a detection efficiency of 2.51 $\pm$ 0.025 % for the ^{137}Cs disk-source through calibration. The relative difference in the coincidence net count rates of ^{90}Sr for the ^{90}Sr disk source and ^{90}Sr + ^{137}Cs disk sources was confirmed to be 0.40 %, which, based on this monitoring system, showed that the radioactivity of nuclides could be separated sufficiently even if beta and gamma nuclides are mixed. The integrated beta/gamma-detection monitoring system developed in this study was indicated to have the potential to provide the foundation for real-time in-situ monitoring in water environments, including groundwater at decommissioning sites.

CRediT authorship contribution statement

Woo Nyun Choi: Writing – original draft, Software, Conceptualization. **Min Ji Kim:** Writing – review & editing, Investigation, Data curation. **Hyeonmin Lee:** Software, Methodology. **Seungbin Yoon:** Formal analysis. **Hee Reyoung Kim:** Project administration.

Declaration of competing interest

The authors declare that they have no known competing financial interests or personal relationships that could have appeared to influence the work reported in this paper.

Acknowledgments

This work was supported by the Korea Institute of Energy Technology Evaluation and Planning and the Ministry of Trade, Industry, and Energy of the Republic of Korea (grant no. 20214000000410).

References

[1] S. Richards, T. Frye, J. Shepherd, T. Nicholson, G. Kuzo, U. Shoop, S. Sakai, R. Allen, Liquid Radioactive Release Lessons Learned Task Force Final Report, Washington D.C U.S, 2006.
[2] Nuclear Energy Institute, Industry Ground Water Protection Initiative-Final Guidance Document, 2007. NEI 07-07. Washington D.C U.S.
[3] Nuclear Safety and Security Commission Notice, No. 2017–17, regulation on environmental radiological surveillance and environmental radiological impact assessment around nuclear facilities. Nuclear Safety and Security Commission, 2017.
[4] J.M. Lim, G.S. Choi, Y.H. Cho, The Annual Report on the Environmental Radiological Surveillance and Assessment Around the Korea Atomic Energy Research Institute (2020) (No. KAERI/RR4687/2021), Korea Atomic Energy Research Institute, 2021.
[5] W.N. Choi, U. Lee, J.W. Bae, H.R. Kim, Minimum detectable activity of plastic scintillator for in-situ beta measurement system in ground water, Nucl. Eng. Technol. 51 (4) (2019) 1169–1175, https://doi.org/10.1016/j.net.2019.02.001.
[6] U. Lee, W.N. Choi, J.W. Bae, H.R. Kim, Fundamental approach to development of plastic scintillator system for in situ groundwater beta monitoring, Nucl. Eng. Technol. 51 (7) (2019) 1828–1834, https://doi.org/10.1016/j.net.2019.05.006.
[7] Eljen Technology. General Purpose EJ-200, EJ-204, EJ-208, EJ-212. eljentechnology.Com/products/plastic-Scintillators/ej-200-Ej-204-Ej-208-Ej-212.
[8] Hamamatsu, Photomultiplier Tube R878. https://www.hamamatsu.com/jp/en/product/opticalsensors/pmt/pmt_tube-alone/head-on-type/R878.html.
[9] G.F. Knoll, Radiation Detection and Measurement, John Wiley & Sons, 2010.
[10] C. Rozsa, R. Dayton, P. Raby, M. Kusner, R. Schreiner, Characteristics of scintillators for well logging to 225 degrees C, IEEE Trans. Nucl. Sci. 37 (1990) 966–971, https://doi.org/10.1109/23.106744.
[11] M. Yoneyama, J. Kataoka, M. Arimoto, T. Masuda, M. Yoshino, K. Kamada, Y. Usuki, Evaluation of GAGG: Ce scintillators for future space applications, J. Instrum. 13 (2018) 02023.
[12] H.Y. Lee, J.A. Jeon, K.W. Kim, W.K. Kim, H.S. Lee, M.H. Lee, Scintillation characteristics of a NaI (Tl) crystal at low- temperature with silicon photomultiplier, J. Instrum. 17 (2022) 02027, https://doi.org/10.1088/1748-0221/17/02/P02027.
[13] Y. Hou, S. Liu, H. Yuan, Q. Gui, C. Zhang, Z. Fang, M. Zhang, Study on high-temperature performance of $LaBr_3$ (Ce) scintillators, in: IOP Conference Series, IOP Conf. Ser.: Mater. Sci. Eng, vol. 678, IOP Publishing, 2019, p. 678, https://doi.org/10.1088/1757-899X/678/1/012084, 1, p. 012084.
[14] W. Drozdowski, P. Dorenbos, A.J.J. Bos, G. Bizarri, A. Owens, F.G.A. Quarati, $CeBr_3$ scintillator development for possible use in space missions, IEEE Trans. Nucl. Sci. 55 (2008) 1391–1396, https://doi.org/10.1109/TNS.2007.908579.
[15] C.J. Werner, MCNP User's Manual-Code Version 6.2, Los Alamos National Laboratory, 2017.
[16] J.C. Hsu, Y.S. Chiang, Y.S. Ma, Photoluminescence and anti-deliquesce of cesium iodide and its sodium-doped films deposited by thermal evaporation at high deposition rates, in: Opt. Compon. Mater., X, vol. 8621, SPIE, 2013, https://doi.org/10.1117/12.2002308.
[17] Ortec Inc., High voltage power supply operating and service manual. https://www.ortec-online.com/-/media/ametekortec/manuals/5/556-mnl.pdfModel556.
[18] Ortec Inc., Dual spectroscopy amplifier operating and service manual. https://www.ortec-online.com/-/media/ametekortec/manuals/8/855-mnl.pdfModel855.
[19] Ortec Inc., Timing single-channel analyzer operating and service manual. https://www.ortec-online.com/-/media/ametekortec/manuals/5/551-mnl.pdfModel551.
[20] Ortec Inc., Time-to-amplitude converter single-channel analyzer operating and service manual. https://www.ortec-online.com/-/media/ametekortec/manuals/5/567-mnl.pdfModel567.
[21] J.H. Ely, C.E. Aalseth, J.I. McIntyre, Novel beta-gamma coincidence measurements using phoswich detectors, J. Radioanal. Nucl. Chem. 263 (2005) 245–250, https://doi.org/10.1007/s10967-005-0044-y.
[22] Ortec Inc., EASY-MCA-2KTM digital gamma-ray spectrometer User's manual. https://www.ortec-online.com/-/media/ametekortec/manuals/e/easy-mca-mnl.pdf.
[23] E. Emsl, Method 900.0: gross alpha and gross beta radioactivity in drinking water. Prescribed Procedures for Measurement of Radioactivity in Drinking Water, 1980. EPA/600/4/80/032.